Invited Review

Collagen Structure: The Molecular Source of the Tendon Magic Angle Effect

Gary D. Fullerton, PhD,* and Andrés Rahal, MD

This review of tendon/collagen structure shows that the orientational variation in MRI signals from tendon, which is referred to as the "magic angle" (MA) effect, is caused by irreducible separation of charges on the main chain of the collagen molecule. These charges are held apart in a vacuum by stereotactic restriction of protein folding due in large part to a high concentration of hydroxyproline ring residues in the amino acids of mammalian collagen. The elevated protein electrostatic energy is reduced in water by the large dielectric constant of the highly polar solvent ($\kappa \sim 80$). The water molecules serve as dielectric molecules that are bound by an energy that is nearly equivalent to the electrostatic energy between the neighboring positive and negative charge pairs in a vacuum. These highly immobilized water molecules and secondary molecules in the hydrogen-bonded water network are confined to the transverse plane of the tendon. Orientational restriction causes residual dipole coupling, which is directly responsible for the frequency and phase shifts observed in orientational MRI (OMRI) described by the MA effect. Reference to a wide range of biophysical measurements shows that native hydration is a monolayer on collagen $h_m = 1.6$ g/g, which divides into two components consisting of primary hydration on polar surfaces $h_{pp} = 0.8$ g/g and secondary hydration $h_s = 0.8$ g/g bridging over hydrophobic surface regions. Primary hydration further divides into side-chain hydration $h_{psc} = 0.54$ g/g and main-chain hydration $h_{pmc} = 0.263$ g/g. The main-chain fraction consists of water that bridges between charges on the main chain and is responsible for almost all of the enthalpy of melting $\Delta H = 70$ J/g-dry mass. Main-chain water bridges consist of one extremely immobilized Ramachandran water bridge per tripeptide $h_{R\alpha} = 0.0658$ g/g and one double water bridge per tripeptide $h_{dwb} = 0.1974$ g/g, with three water molecules that are sufficiently slowed to act as the spin-lattice relaxation sink for the entire tendon.

Key Words: tendon; collagen; hydration; water binding; protein hydration; collagen hydration; bound water; magic angle effect; water bridges; double water bridges; T1 relaxation; T2 relaxation; MRI contrast phenomena
J. Magn. Reson. Imaging 2007;25:345–361.

THIS REVIEW OF BIOPHYSICAL STUDIES of mammalian tendon extends beyond the MR literature to show how the molecular structure of the collagen molecule causes the highly exceptional variation of MR signal with tendon orientation in the magnetic field that is referred to as the "magic angle" (MA) effect (1–14). Tendon is a unique tissue for elucidating not only orientational effects but also the molecular sources of MR contrast in other tissues. The unique "Rosetta stone" character of tendon relates to four structural factors:

1. The nearly monomolecular composition of tendon, in which the collagen content approaches 100% of the total dry mass in some instances.
2. The uniform parallel alignment of collagen molecules along the tendon long axis, which provides tensile strength for connecting muscles to bones and forming cables necessary for mechanical motion of the body.
3. The quasi-crystalline association of collagen molecules in tendon, which allows the application of x-ray crystallography methods to both synthetic collagen crystals and native tendon.
4. Immobilization of the stiff collagen molecule, which causes dipole-dipole coupling of protons in the collagen molecule to suppress signal originating from the protein itself and ensures water-only MRI signals with relaxation dominated by water motion.

In this review we summarize the collagen structural information that has been derived from x-ray diffraction studies over the past century, embarking from a historical review of early work by Rich and Crick (15). The collagen structure provides the molecular model of collagen hydration that is necessary to understand MRI signal and contrast. Molecular hydration predicts hydration fractions (h(g/g)) in grams of water per gram of dry mass using the assumption that dry mass is exclusively collagen. Three hydration fractions are identified with categorical differences in immobilization due to differences in free energy of water binding. Comparisons of model predictions with biophysical studies of tendon confirm both the size of the water compartments and the categorical changes in water molecule mobility. Compartmental immobilization of water on collagen is shown to cause T1 variation with tissue hydration due to fast exchange between highly immobilized primary hydration on the collagen main chain

Radiology Department, University of Texas Health Science Center at San Antonio, San Antonio, Texas, USA.
*Address reprint requests to: G.D.F, Department of Radiology, University of Texas HSCSA, 7703 Floyd Curl Drive, San Antonio, TX 78229. E-mail: fullerton@uthscsa.edu
Received April 19, 2006; Accepted September 12, 2006.
DOI 10.1002/jmri.20808
Published online in Wiley InterScience (www.interscience.wiley.com).

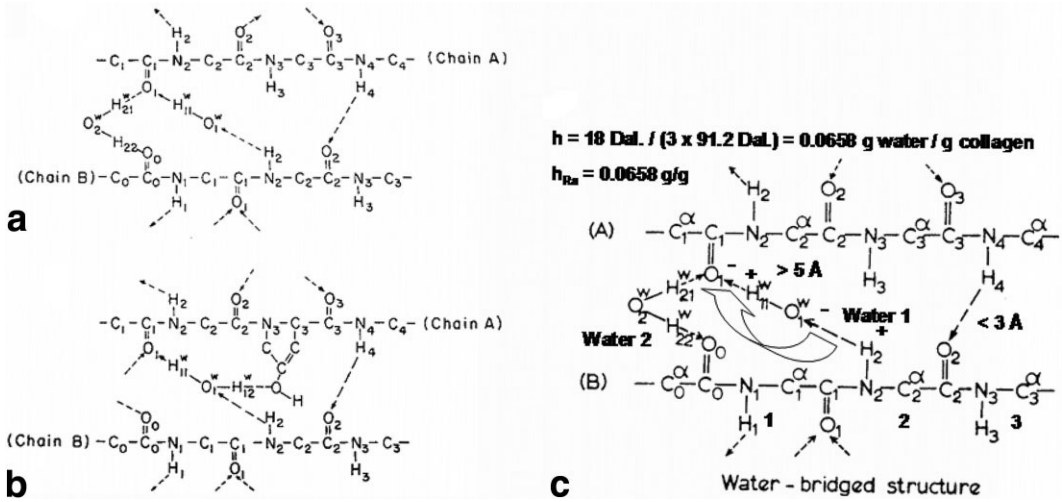

Figure 1. The initial Rich and Crick (15,16) single hydrogen bond per tripeptide (A chain-N_4H_4 to B-chain C_2O_2) collagen model was modified by Ramachandran to include two bonds per tripeptide (20). One direct A-chain hydrogen bond per tripeptide and one water bridge (B chain-N_2H_2 to A-chain C_1O_1) was necessary to complete the two-bond model proposed by his group. **a:** The configuration when B-chain peptide 3 is other than hydroxyproline. **b:** The configuration when tripeptide includes hydroxyproline in position 3. **c:** The role of the water bridge in transferring charge to reduce the electrostatic free energy due to the high dielectric constant of water $\kappa = 80$. In both instances the Ramachandran water bridge hydration $h_{Ra} = 18$ Da/(3 × mean peptide molecular weight) = 0.0658 g/g for collagen. Reprinted from Fullerton GD, Nes E, Amurao M, Rahal A, Krasnosselskaia L, Cameron I. An NMR method to characterize multiple water components on mammalian collagen. Cell Biol Int 2006;30:66–73, with permission from Elsevier.

with less immobilized surface water fractions. Preferential orientation of the water electric dipole in the transverse plane of the collagen molecule has been shown to be the primary cause of orientational T2/T2* variation, which is referred to as the MA effect in the MRI literature. MRI images of tendon demonstrate a correlation between molecular prediction and image contrast with extensions to describe pathologies that directly attack the molecular structure of collagen.

STRUCTURAL X-RAY DIFFRACTION STUDIES OF COLLAGEN

X-Ray diffraction on crystal lattices of biological materials, such as tendon and crystalline collagen, were first reported in the 1920s and reviewed in the seminal report by Rich and Crick (15). Tendon was among the earliest tissue studies using improved methods in the middle of the 20th century. Sir Francis Crick (who is better known for his work with James Watson on DNA) worked on deriving the triple helix structure of collagen. Rich and Crick (15,16) proposed a triple helix structure with a single hydrogen bond for every three protein residues, as shown in Fig. 1. A second group in India directed by Ramachandran and Kartha (17,18) proposed a second bond per tripeptide group, which resulted in a controversy between proponents of the one-bond model vs. those who favored the two-bond model. Ramachandran modified the two-bond model in response to criticism from Rich and Crick, who noted that

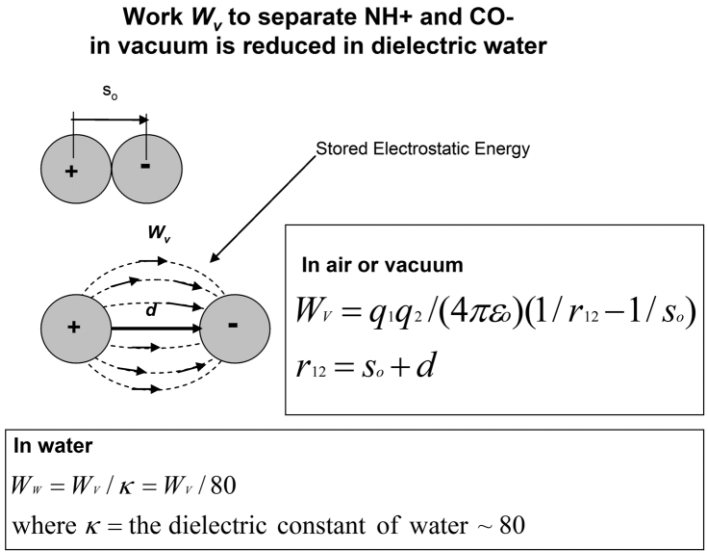

Figure 2. The partial electron charge on the positive amide ($q_1 \sim +0.3\ q_e$) and the negative carbonyl ($q_2 \sim -0.3\ q_e$) are held a distance d apart by conformational folding restrictions of the protein chain as described by the well-known Ramachandran plots. When the protein is immersed in water, the free energy is reduced by a factor $1/\kappa$ (one over the dielectric constant) or approximately 1/80 due to alignment of water electric dipoles. The electrostatic energy differential creates a free energy well that holds the water bound to the protein between the charged regions, where the enthalpy is $\Delta H = W_V - W_W = 79/80$, $W_V = 0.988\ W_V$, and the Gibbs free energy is $\Delta G = \Delta H - T\Delta S$. At the melting temperature T_m, where $\Delta G = 0$, one calculates the change in entropy $\Delta S = \Delta H/T_m$ that occurs when water molecules are liberated from the aligned position on the collagen, causing a large increase in motional energy. Entropic changes are almost entirely due to surface water because the collagen molecules are stiff with limited mobility.

the charge separation was too large to allow the second hydrogen bond. In 1968 Ramachandran and Chandrasekharan (20) proposed the insertion of a water bridge to resolve the problem (19,21,22). The existence of water bridges was confirmed by Yee et al. (23) using tritiated proton exchange experiments, and later by Burjanadze using phylogenetic comparisons (24). The hydration for the Ramachandran bridge of one water for three residues is $h_{Ra} = 18/(3 \cdot 91.2) = 0.0658$ g/g.

Main-Chain Water Bridges

In retrospect, one can see that the formation of water bridges can be explained by basic electrostatic physics. As shown in Fig. 2, two oppositely charged particles separated in space require work of formation stored in the electric field between them. The energy is calculated from the work done to move charges from the minimum energy state in direct contact to the higher-energy state separated by the distance d. The large separation of the NH^+ and CO^- noted by Rich and Crick implies a higher electrostatic energy. The Rich/Crick direct hydrogen bond serves as the reference point or lowest energy state for such a charge pair. The Ramachandran water bridge bond has large separation d due to the inability of the protein chain to fold further. When the molecule is placed in water with a dielectric coefficient of $\kappa \sim 80$, the electrostatic energy is reduced by the factor 79/80 to within a few percent of the reference state of the direct hydrogen bond. This creates a free energy well that holds the water molecule in place, as shown in Fig. 3. Since the water bridge is intramolecular between α-chains and locked between the nearest amide and carbonyl groups, the electric dipole is confined to the transverse plane relative to the molecular long axis. High-resolution studies of collagen analogs confirm that the carbonyl groups of glycine are singly hydrated (25) in the Ramachandran bridge. The carbonyl groups on proline residues in the Y position are, however, doubly hydrated to form double water bridges.

Main-Chain Double Water Bridges

The single remaining NH^+/OH^+ in the fundamental tripeptide structure of collagen is too distant from negatively charged carbonyl groups to form a Ramachandran water bridge. In a vacuum, however, the electrostatic energy of the separated positive amide and neighboring negative carbonyl groups is even larger than the Ramachandran bridge due to the increased separation d. Immersion in water reduces the energy by insertion of a longer water bridge, which by symmetry one can predict to be the next longest or a double water bridge, as shown in Fig. 4. The double water bridge involves three water molecules with one molecule bound to the amide and two additional water molecules attached and branching off to form dendritic paths to nearby carbonyl groups (26). Thus, four water molecules function as (one) single and (three) double water molecule bridges between the solvent-accessible charges on the protein main chain. The water molecules occupy low-energy depressions on the protein surface induced by charge separation. They are immobilized relative to bulk water and aligned in the plane transverse to the axis of the molecule. Water alignment is transverse to the axis of tendon, since collagen molecules are coaxial with the tendon axis in the native state. These predictions are in accord with both biophysical measurements and MR relaxation of water on collagen, as discussed in later sections. The hydration level for cleft water (single water bridge plus double water bridge) is $h = 4 \cdot h_{Ra} = 4 \cdot 18/(3 \cdot 91.2) = 0.263$ g/g.

Formation of Water Sheaths

The ability of water molecules to provide two positive charge donor sites and two negative acceptor sites promotes the formation of hydrogen-bonded polar water networks that cause water to apparently defy gravity by climbing the wall of hydrophilic beakers. This is due to the enthalpy of liberation of water $\Delta H_{lib} = 2.29$ J/mole-water = 123.8 J/g-water at 25°C (27). Berendsen (1) took note of this networking property to propose the formation of water chains attached to hydrogen-bonding sites along the axis of the collagen molecule, as shown in Fig. 5. Lim (28) extended Berendsen's ideas to propose a model of water in the grooves of the collagen molecule, which was used to show that water attached to the main-chain hydrogen bonding sites is filled with four water molecules per tripeptide or $h = 4 \times 18/(3 \cdot 91.2) = 0.2632$ g/g (29). This conclusion agrees with the discussion above regarding single and double water bridges. Using the water network/chain concept that water nearest neighbors must form chains in any measurement direction, Fullerton and Amurao (30) showed that monolayer hydration of collagen requires a chain of 18–20 water molecules to circle the molecule. The hydration of native tendon $h = 18/3 \cdot 0.263$ g/g = 1.6 g/g is barely sufficient to provide monolayer coverage of the solvent-accessible surfaces of the collagen molecule. Thus, native mammalian tendon is covered by a monolayer sheath of water, which agrees closely with recent high-resolution x-ray diffraction studies of collagen analog molecules, in which high-purity crystals, reduced molecular complexity, microgravity crystal growth, and high-intensity synchrotron x-ray irradiation allow sufficient resolution to localize the network of water bridges (31–36) as shown in Fig. 6.

Polar Side-Chain Hydration

As shown later in the section on solvent-accessible surface area (SASA), there is twice as much polar surface or charge sites on the side chain of the amino acids of collagen compared to the main chain. The capacity of side chains to rotate and bend provides sufficient reorientation to reduce the distance d between positive and negative charge sites when the protein is dehydrated. This implies a smaller energy differential between the vacuum (dry) and hydrated states, and very small enthalpy of melting for polar side-chain hydration (see section on thermodynamic properties). The cooperative linking of water molecules bound to the polar side chains with water molecules bound to the main chain of the protein is necessary for the lowest free energy state

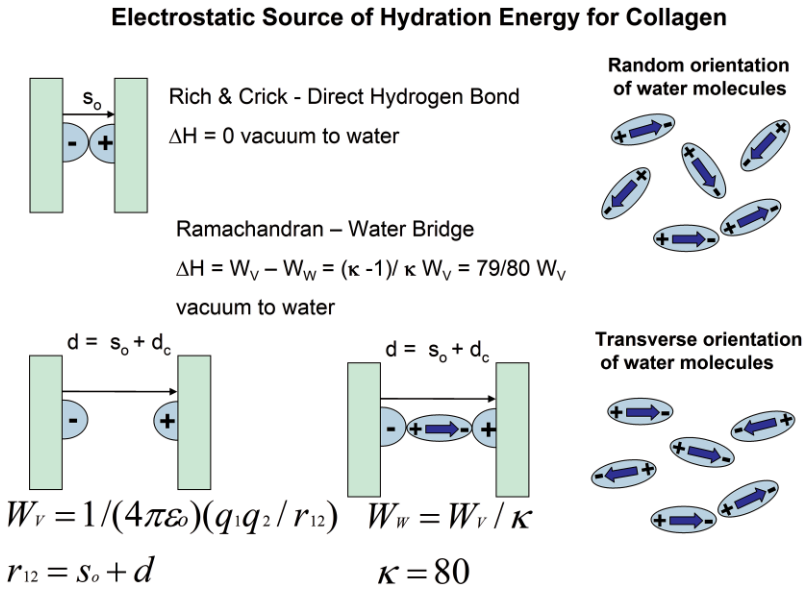

Figure 3. The alignment of the collagen molecule with the direct hydrogen bond described by Rich and Crick (15,16) causes no change in enthalpy when the molecule is immersed in water, but the large separation, which we estimate as the minimum separation required for a water molecule, d_c = 2.35 Å (see Berendsen 1, 2), gives a large change in the enthalpy of melting $\Delta H = W_v - W_w = (\kappa - 1)/\kappa \times W_v = 79/80\ W_v$. Bulk water is randomly oriented; however, on the collagen surface it is confined by service as the molecular dielectric to the plane transverse to the collagen molecule, and as a result of the parallel alignment of the molecules in tendon, the dipoles are also in the transverse plane for tendon. As shown in Figs. 4 and 5, the dipoles occupy a range of orientations about the transverse direction and are slightly misaligned from the orthogonal due to the molecular structure and association of two α1 and one α2 chains. However, the mean orientation in tendon will be orthogonal to the tendon axis due to averaging over large numbers of fibers with random mixtures of molecular misalignments.

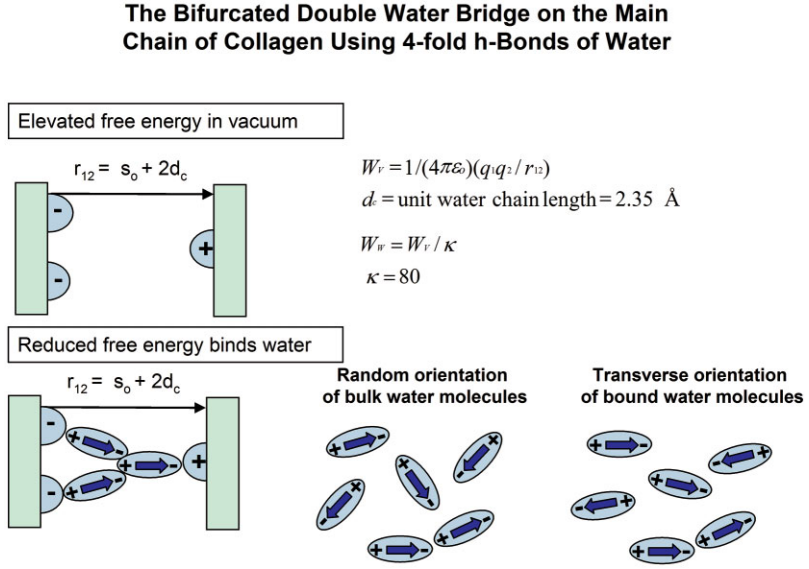

Figure 4. The elevated free energy state of the final amide and carbonyl pair on the tripeptide unit of the protein α-chain following fulfillment of the Rich/Crick direct bond and Ramachandran single water bridge is reduced by completion of a bifurcated double water bridge. The enthalpy of melting for double water bridges can be estimated by assuming that all three charges are equidistant with the separation r_{12} and the same magnitude of partial charge, q = either + or – 0.3 q_e. Using this simplifying assumption, $\Delta H = W_v - W_w = (\kappa - 1)/\kappa; \times W_v = 79/80\ W_v = 79/80\ (W_{--} + W_{+-} + W_{-+}) = 79/80\ W_{+-}$ as $W_{--} = -W_{-+}$, i.e., work is done to separate opposite charge while equal work is done by the pair of like charges during separation. If we further assume that s_o = 4 Å and d_c = 2.35 μ, then the work per mole of bonding sites is 1281 J/mole, which is equivalent to 427 J/mole of water because there are three waters for every double water bridge site. This value agrees well with the direct measurements by differential scanning calorimetry of enthalpy per mass water for bovine and other mammalian tendon, as shown elsewhere in the text regarding the biophysical properties of tendon.

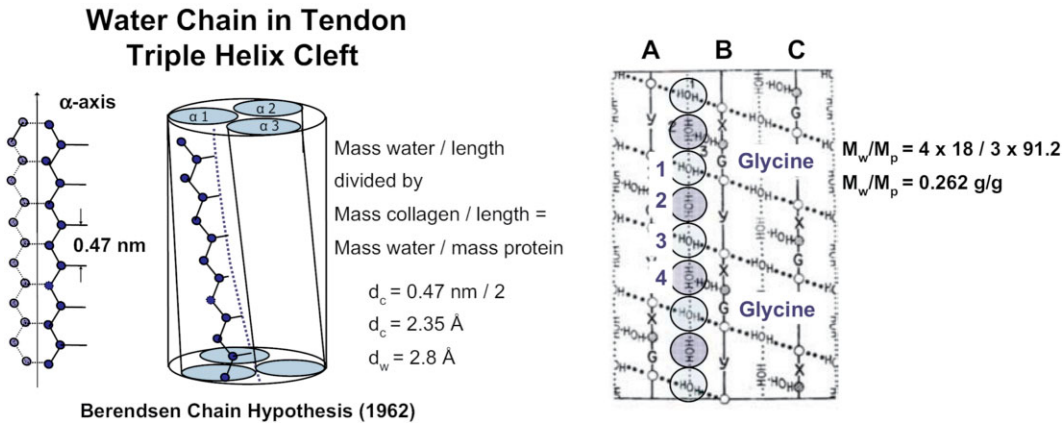

Figure 5. The Berendsen (1) water-chain hypothesis assumes that the water network conforms to ice-like spacing adjusted to room temperature (22°C, as shown at the left) and is useful for calculating geometric relationships for hydrated collagen (30). Berendsen showed that such a water chain matches perfectly with the spacing of hydrogen bonding sites on the collagen main chain with a spacing of 0.47 nm between bonds or d_c = 0.235 nm per water molecule chain link. This model was adapted by Lim (28) to show (drawing on the right adapted from Ref. 28) that there are four water molecules (18 Daltons each) per every three protein residues (mean = 91.2 Daltons each) or 0.2632 g water/g collagen for a single chain of water in each groove or cleft of the collagen triple helix. Reprinted from Fullerton GD, Amurao MR. Evidence that collagen and tendon have monolayer water coverage in the native state. Cell Biol Int 2006;30:56–65, with permission from Elsevier.

because it minimizes the number of unfilled hydrogen bonding sites (enthalpic water change) in a manner similar to that of water on the glass wall of a beaker. Hydration slowly forces side-chain charges apart with little change in free energy. The hydration forms weakly bound intramolecular water bridges between positive and negative charge sites on neighboring collagen molecules. (See Ref. 31 for a detailed description of this hydration network and the section on paradoxical osmotic properties for energy effects.)

Primary and Secondary Hydration

The monolayer water sheath covering the collagen molecule surface consists of the most proximal primary hydration adjacent to polar surfaces and a distal hydration adjacent to hydrophobic surfaces, as shown in Fig. 7. As demonstrated in the studies of Berisio et al (25), the first monolayer of water on collagen consists of nearly half primary hydration and half secondary hydration. The model of native tendon proposes a total monolayer collagen hydration h = 1.6 g/g, half of which is associated with polar surfaces h_p = 0.8 g/g, and the other half of which is associated with hydrophobic or nonpolar surfaces h_n = 0.8 g/g. The mean separation between water molecules and the collagen surface over polar regions according to Berisio et al's measurement (see Fig. 7) is 2.7 Å, while the separation from nonpolar surface is 3.6 Å or 0.9 Å greater. The function of water

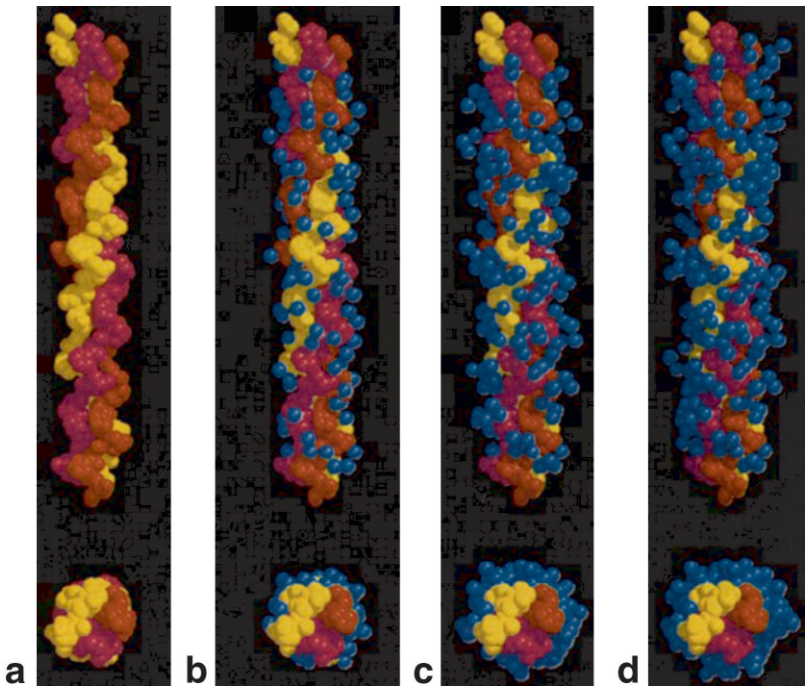

Figure 6. Sequential localization of water molecules during hydration of the collagen-like peptide (Pro-Hyp-Gly)$_4$-Pro-Hyp-Ala-(Pro-Hyp-Gly)$_5$ from Ref. 31, as measured by high-resolution x-ray diffraction measurements on high-purity crystals, shows the formation of the hydration sheath formed by multiple configurations of water bridges between charge sites on the peptide surface. Results are typical for all multiple experiments on a range of collagen analogs. Reprinted from Bella J, Brodsky B, Berman HM. Hydration structure of a collagen peptide. Structure 1995;3:893–906, with permission from Elsevier.

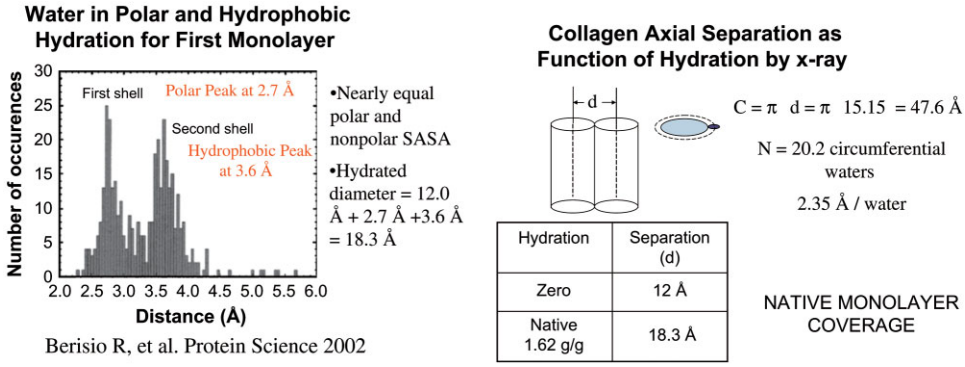

Figure 7. Synchrotron x-ray diffraction measurements of water separation from the collagen surface yield first shell (polar hydration) and second shell (hydrophobic hydration) water separation from the protein surface (25). There are nearly equal amounts of polar and hydrophobic surface, which allows estimation of the mean hydrated diameter (18.3 Å). The circumferential water chain thus has a diameter of 15.1 Å. This yields an estimate of 20.2 water molecules in the circumferential water chain, in good agreement with other calculation methods (30). Reprinted from Fullerton GD, Amurao MR. Evidence that collagen and tendon have monolayer water coverage in the native state. Cell Biol Int 2006;30:56–65, with permission from Elsevier.

as the dielectric to reduce the electrostatic energy implies that polar portions of the surface will be hydrated first followed by bridge hydration over the hydrophobic regions when $h > 0.8$ g/g.

SASA

It is generally thought that one of the primary functions of protein folding is to reduce the hydrophobic surface area of the protein exposed to water. This contributes an entropic term to the energetics of folding as hydrophobic surfaces restrict water motion by limiting acceptable orientations of the water, and thus allowing formation of hydrogen bonds. Fullerton and Amurao (30) used the method of Miller et al (37,38) to calculate the SASA for collagen and demonstrated that a large fraction of the hydrophobic surface is sequestered for native collagen, as shown in Table 1. The h_{max} is the theoretically calculated maximum possible hydration with full extension of the protein molecular chain and no steric restrictions, and h_{nat} is the native water fraction in each component after folding into α-chains and winding into the triple helix. The h_{dis} is the water displaced by folding or self-association. It is assumed that all polar surfaces are hydrated except for the portions on the main chain, where 0.26 g/g are displaced by one Ramachandran water bridge per tripeptide and one direct hydrogen bond as described by Rich and Crick (15,16) (see Ref. 30 for details). As shown in Table 1, 83% of the sequestered surface is hydrophobic. In addition, the native hydration fractions are consistent with the conclusions concerning primary and secondary hydration. The hydration of native tendon/collagen is summarized in Fig. 8.

Table 1
Calculation of Collagen Solvent Accessible Surface (SAS) Areas and Relation to Monolayer Hydration Fractions for Polar, Nonpolar, and Total Coverage

Surface	SAS_{max}(Å^2)	h_{max}(g/g)	h_{dis}(g/g)	h_{nat}(g/g)
Polar	205218	1.06	**0.26 (17%)**	0.8 (50%)
Nonpolar	402197	2.07	1.25 (83%)	0.8 (50%)
Total	607416	3.13	1.53 (100%)	**1.6 (100%)**

Bold indicates directly measured values, while others are calculated.

BIOPHYSICAL PROPERTIES CORRELATE WITH STRUCTURAL HYDRATION

The clarification of a molecular model of collagen hydration discussed above shows that tendon has monolayer water coverage with a network of water bridges with either direct primary hydrogen bonding to the protein or a secondary bonding through a primary water molecule. A wide variety of experiments on tendon and collagen have confirmed paradoxical water properties using optical (39,40), isothermic (41), calorimetric (41,42), NMR orientational (3,4,14), and NMR titration (43) methods. The molecular model suggests that biophysical properties of native tendon are strongly dependent on water content. We selected three types of studies from the extensive literature to clarify the predictions and provide the basis for relating NMR relaxation properties and MRI contrast of tendon to molecular properties. The narrowed range includes: 1)

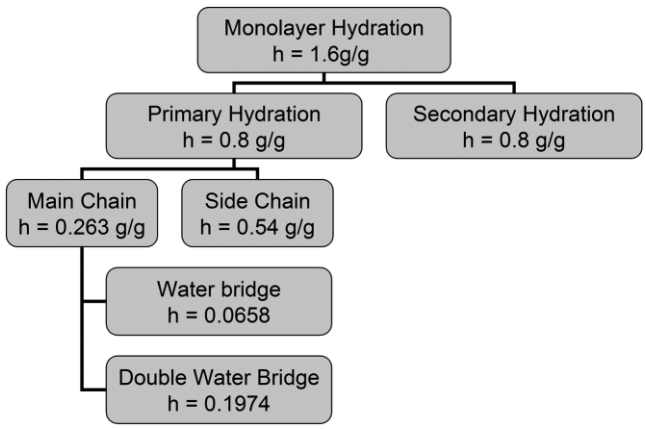

Figure 8. Summary of the monolayer hydration compartments of native tendon/collagen.

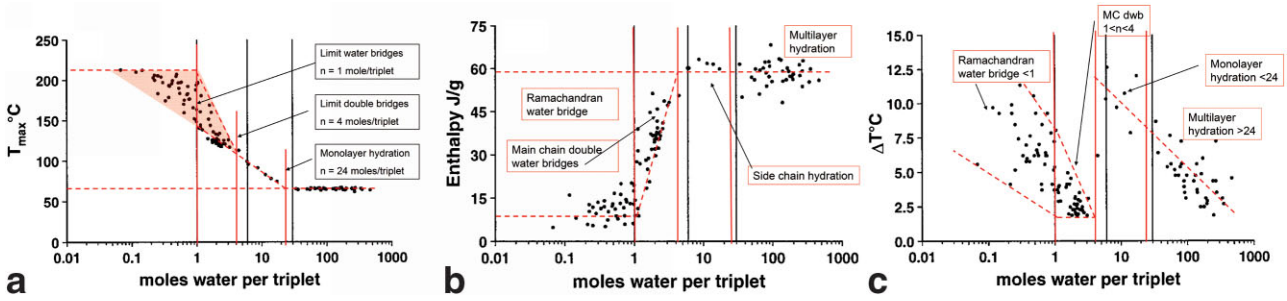

Figure 9. Study of the melting of rat tail tendon (45) by differential scanning calorimetry shows that the temperature peak of melting depends on the level of hydration as described by molecular hydration model predictions. The vertical red lines from the collagen hydration model added in the present work show agreement with the empirical placement of compartment limits by Miles and Ghelashvili (45), indicated with black lines. **a:** The T_{max} = 65.1°C for all hydration levels greater than $N > 24$, where the first monolayer coverage h = 1.62 g/g. The melting temperature is a monotonic function of hydration when $h > 0.26$ g/g or four water molecules per triplet. Below four, the T_{max} varies within the shaded range due to formation of steam when water is released from the collagen ($T_{max} > 100$°C) to cause a highly variable pressure volume (PV) enthalpy term related to variability in capsule expansion and seal effectiveness. **b:** The enthalpy is a linear function of hydration between 1 and 4 moles of water per triplet. It is constant in the Ramachandran water bridge region below 1 where enthalpy ΔH(J/g) = 11.6 J/g, and above 4 where ΔH(J/g) = 62 J/g. The slope in the double water bridge (dwb) region (62–11.6)J/g/(0.26–0.065)g/g gives a direct measurement of the enthalpy contribution of the bound dielectric water ΔH(J/g-water) = 255 J/g-water, which for comparison is about 75% of the enthalpy of melting ice water at 0°. **c:** There is a sharp demarcation in the width of the melting peak at hydration 4 moles/triplet. Above 4 the width reflects the presence of two peaks: the low temperature peak due to side-chain hydration, and the high temperature peak due to main-chain hydration. The peak narrows as the contribution of main-chain hydration becomes small relative to the side-chain population. Below hydration 4 moles/triplet, the peak width is highly variable due to variable PV terms caused by steam. Modified from Miles CA, Ghelashvili M. Polymer-in-a-box mechanism for the thermal stabilization of collagen molecules in fibers, Biophys J 1999;76:3243–3252, with permission.

thermodynamic studies of collagen/tendon melting energetics to clarify the changes in water motion among the three categories of water in the first monolayer, 2) optical relaxation studies that clearly demonstrate the orientational restriction of water molecules that are responsible for the MA effect, and 3) biomechanical studies of tendon that demonstrate a relation between patient tissue properties and MRI-observable changes.

Thermodynamic Properties of Collagen Hydration Compartments

The extensive literature covering studies of the thermodynamic properties of tendon and collagen as reviewed and summarized in Ref. 44 is recommended as a starting point for the interested reader. Early studies of the dependence of the enthalpy of heating on the hydration level show strong dependence on primary hydration range and reduced importance for secondary hydration (41,42). More recent studies by Miles and Ghelashvili (45) (see Fig. 9) are typical of the studies that demonstrate the capacity of the molecular hydration model to predict aspects of biophysical response. The collagen molecular hydration model is consistent with differential scanning calorimetry (DSC) measurements of collagen melting. In addition, the conversions of enthalpy of melting per dry collagen mass to enthalpy of melting per mass water ΔH(J/g-water) = 255 J/g-water gives a value that is in reasonable agreement with ΔH(J/g-water) = 470 J/g-water calculated with the simplified model described in Fig. 4.

Axial Dilation With Hydration

Fullerton and Amurao (30) used a comparison of hydration-induced tendon diameter expansion as a function

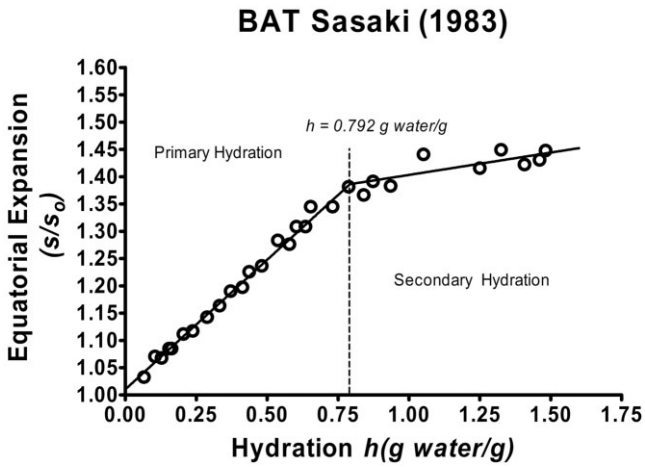

Figure 10. A reevaluation of the BAT data from Ref. 46 shows that equatorial expansion of tendon measured by x-ray diffraction has significantly higher slope in the "primary hydration" phase, in which water covers polar sites at the initial low hydration levels, than the much smaller slope in the "secondary hydration" range. Primary hydration fills first due to lower Gibbs free energy, as described above. Secondary hydration occurs at higher hydration levels and is sometimes referred to as the "disappearing water fraction" because the apparent volume occupied by this water is much less than the volume increase for primary hydration. Secondary hydrations bridge over hydrophobic regions by hydrogen bonding to primary hydration water molecules, and settle into the cracks left by the protruding primary hydration molecules (see Ref. 30 for details). The regression fit to the bimodal model has a goodness of fit r^2 = 0.992 for 29 values and 26 degrees of freedom. The change in slope at $h \sim 0.8$ g/g indicates good agreement with the monolayer hydration of native tendon. Reprinted from Fullerton GD, Amurao MR. Evidence that collagen and tendon have monolayer water coverage in the native state. Cell Bio Int 2006;30:56–65, with permission from Elsevier.

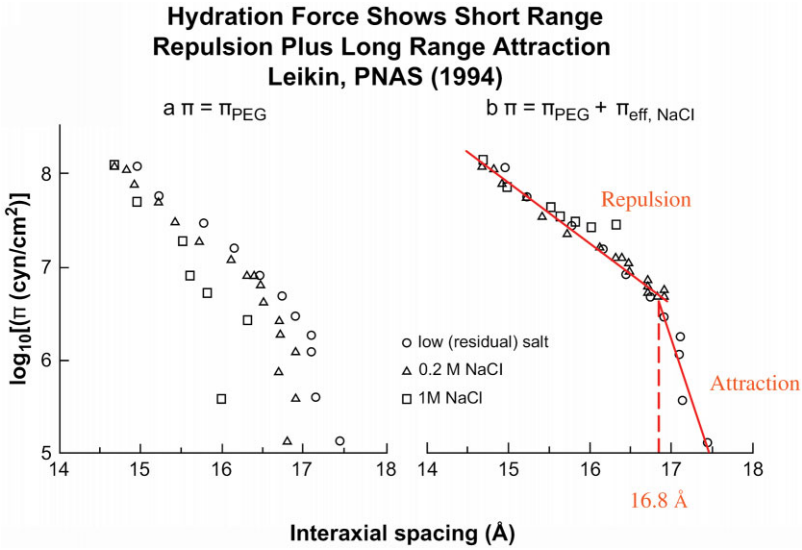

Figure 11. In a hydration force experiment on rat tail tendon, Leikin et al (88) applied osmotic compression to collagen by submersing the tendon in a water solution of inert PEG, which because of the large size of the PEG molecule (MW = 8000Da) cannot penetrate into the interaxial spaces between the collagen molecules. Exclusion of PEG creates an osmotic pressure. The concentration of PEG is converted to osmotic pressure (dynes/cm^2) using an empirically measured relationship (49) and plotted on a log scale to encompass pressures over three orders of magnitude. The pressure is plotted as a function of collagen interaxial spacing calculated from equatorial spacing measured by x-ray diffraction. As shown on the right, when a partial exclusion of salt is accounted for, a single curve can describe the results at all salt concentrations (88). The results describe repulsion for separations less than 16.8 Å and attraction for larger separations. Since the sum of the diameter of dry collagen 12.1 Å (88,89) and Berendsen double water separation 4.74 Å (90) (see Fig. 5) is 16.8 Å, the break between attraction and repulsion occurs at the level of monolayer hydration. Less than monolayer hydration causes repulsion due to the reduced energy of the hydration sheath (see text for discussion). Collagen at larger separations experiences an attraction that reduces the entropy of dielectric water bridging between charges by reducing separation between charges. Reprinted from Fullerton GD, Amurao MR. Evidence that collagen and tendon have monolayer water coverage in the native state. Cell Biol Int 2006;30:56–65, with permission from Elsevier.

of hydration h(g/g) to prove tendon expansion as predicted from axial molecular separation measurement using x-ray diffraction. This extends to native tendon hydration to prove that mammalian tendon has only monolayer surface water coverage. Furthermore, a re-evaluation of the data from Ref. 46 on bovine Achilles tendon (BAT), as shown in Fig. 10, shows that approximately half of the native hydration h_{na} = 1.6 g/g is secondary hydration over hydrophobic surfaces h_{sec} = 0.8 g/g, while the remaining half is primary hydration

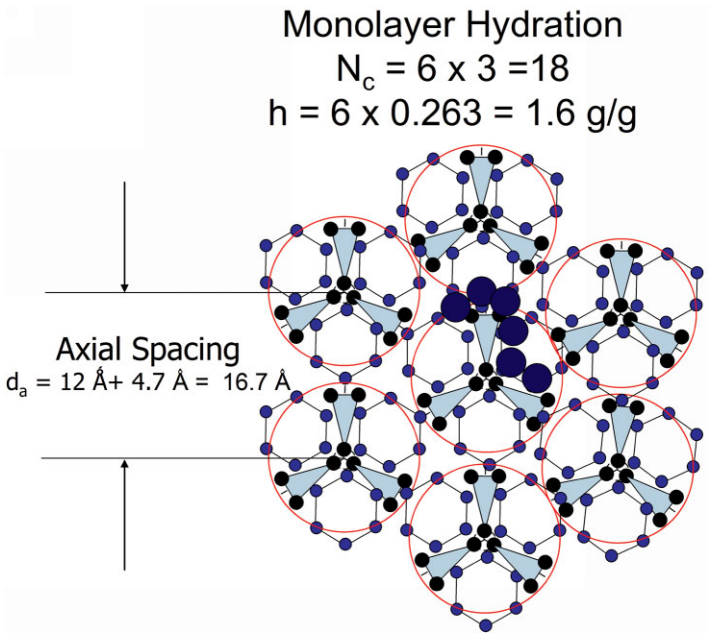

Figure 12. A cartoon of native tendon (30) demonstrates several important concepts related to native hydration. Black dots represent c_α carbons of the collagen amino acids, and blue dots represent water molecules. With N_c = 18 parallel water chains: 1) monolayer coverage provides nearest neighbors for all water molecules to maintain four-bond geometry of bulk water; 2) a single chain of water per groove provides h = 0.263 g/g, while six chains per groove with h = 1.6 g/g is necessary to circumscribe the molecule for native tendon hydration; and 3) monolayer hydration increases the dry axial separation of 12 Å by 2 d_c = 4.7 Å to a fully hydrated axial separation 16.7 Å, as shown by the hydration force experiment of Leikin (88). Reprinted from Fullerton GD, Amurao MR. Evidence that collagen and tendon have monolayer water coverage in the native state. Cell Biol Int 2006;30:56–65, with permission from Elsevier.

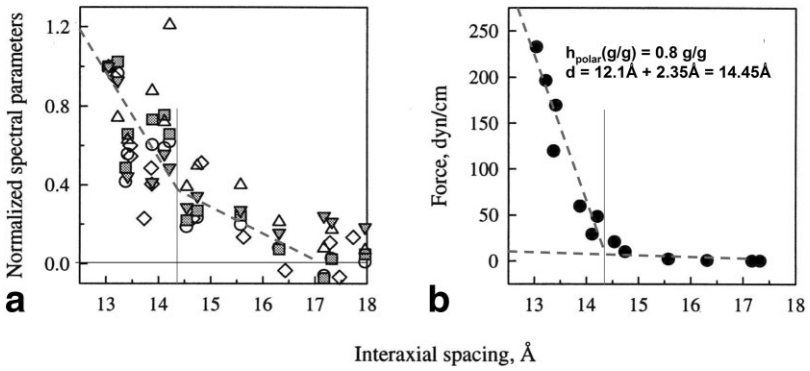

Figure 13. a: Normalized Raman spectroscopy factors of relative peak intensity and spectral shift for the OH bands and NH peak half width plotted on the same normalized scale on collagen as a function of hydration *h*(g/g) as measured by interaxial spacing. The parameters were linearly scaled by Leikin et al (39) to be zero in bulk water (for the NH half-width a hydrogen/deuterium exchange experiment, the value was zero), and 1.0 refers to the sample that contains the least amount of water. **b:** Intermolecular hydration force measurements for the same samples. Both data sets show distinct changes in slope at the interaxial spacing predicted for filling all polar bonding sites, $h = 0.8$ g/g. Separation at this hydration would be 12.1 Å (dry collagen diameter) plus 2.35 Å (half the monolayer hydration or the single effective water diameter described by Berendsen (1)) equals 14.45 Å. The optical measures confirm bonding to the OH and NH groups, while the expansion confirms that water causes the changes. The vertical lines were added in the present work to highlight the breakpoint at the border between primary and secondary hydration predicted by the hydration model. Modified from Leiken S, Parsegian VA, Yang W, Walrafen GE. Raman spectral evidence for hydration forces between collagen triple helices. Proc Natl Acad Sci USA 1997;94:11312–11317, with permission of National Academy of Sciences, USA.

covering both main- and side-chain polar surfaces $h_{pri} = 0.8$ g/g. This agrees with the division of primary and secondary hydration on collagen analogs measured directly with high-resolution x-ray diffraction (25).

Paradoxical Osmotic Properties of First Monolayer Water

Comparisons of the water content of tendon $\%H_20 = 1.6/(1 + 1.6) = 61.6\%$ shows that the water content is consistent with the water content of cells without the presence of a membrane or a pump mechanism to maintain the water content. Water on tendon has paradoxical properties similar to those reported for cellular water (47,48). On collagen, the high water content is due to hydration of positive and negative charges held apart by the limited conformational freedom of the protein main chain. The reduced activity of surface water is best studied with hydration force experiments using mechanical or osmotic compression with a large, nonpenetrating cosolute, such as 20 kDa polyethylene-glycol (PEG) (49). Hydration force experiments show that collagen interfacial water has reduced free energy relative to bulk water, but can be removed by the application of osmotic stress or mechanical stress (39,50–53), as shown in Fig. 11. These measurements confirm that large repulsive forces hold collagen molecules apart separated by two layers of water between molecules. Figure 12 shows that monolayer water coverage of the tendon has fourfold hydrogen bonding typical of bulk water while also networking to all hydrophilic sites of the protein structure.

Optical Evidence of Water Bonding to NH and CO

Early optical evidence of water attachment to NH and CO groups on collagen was first summarized in the monograph on collagen edited by Ramachandran (54). It was shown by dichroic measurements that NH and CO bonds are essentially perpendicular to the tendon axis (40), confirming the orientational conclusions of Figs. 3 and 4. The results of a Raman spectrum study of OH and NH bond vibrational bands (39) confirm that water is bonding to these groups, as shown in Fig. 13, and that the perturbation is greatest for $h < 0.8$ g/g, where direct primary hydration occurs but continues with less influence over the secondary hydration range between $h = 0.8$–1.6 g/g, where water bridges between primary hydration water molecules. Leikin (39) used the relative intensity of the OH bands to calculate the binding energy of tightly bound water relative to bulk water. He estimated 1 kcal/mole, which compared well with his direct osmotic work measurement of 60 cal/cm^3. Converting both values to units of J/g-water gives an optical estimate of 232 J/g and an osmotic work measurement of 251 J/g, both of which compare well with the 255 J/g calculated earlier from the DSC measurement by Miles and Ghelashvili (45). All three values agree with the estimated electrostatic energy calculation of Fig. 4 and lend further support to the conclusions derived from the molecular hydration model.

Mechanical Properties of Tendon and Hydration

The biomechanical or rheological characteristics of tendon require extension beyond molecular characteristics of collagen to include the hierarchy of structural categories shown in Fig. 14. Although the biomechanical response of tendon has an important dependence on the entire hierarchy of structural relationships (55), a subset is directly related to colla-

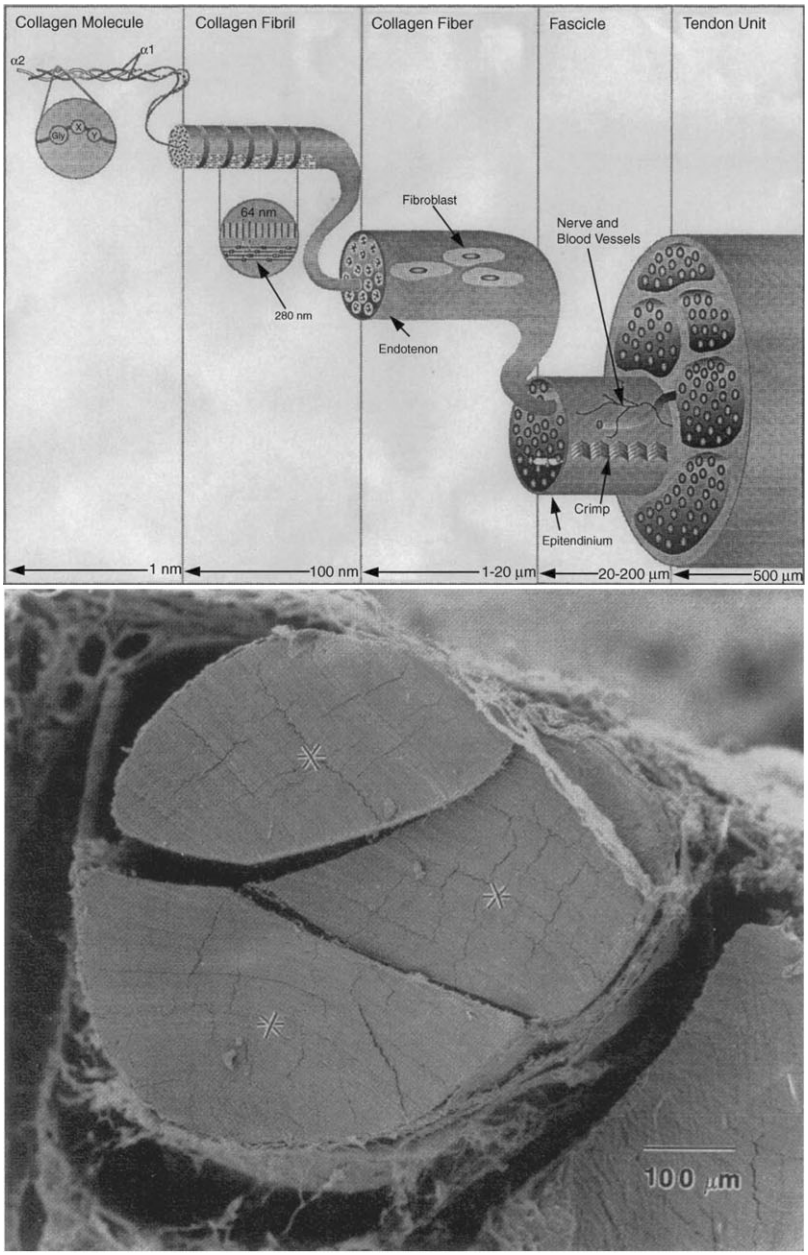

Figure 14. This diagram shows the hierarchical structure of tendon proceeding from the molecular collagen to formation of fibrils, fibers, and fascicles to tendon units. This illustrates the many levels of organization that we can ignore in some experiments due to the high concentration of collagen. Mechanical properties depend more on the macrostructure that is visible in this example of a scanning electron micrograph of rat tail tendon showing fascicle units (asterisks) that make up the tendon. Reprinted from Silver FH, Freeman JW, Seehra GP. Collagen self-assembly and the development of tendon mechanical properties. J Biomech 2003;36:1529–1553, with permission from Elsevier.

gen hydration properties. As shown in Fig. 15, when tendon is subjected to stress (force/area) it will stretch with a strain ($\Delta l/l$) that is nonlinear with stress. However, the toe and heel regions are completely eliminated when the water is removed (56). MR measures of apparent diffusion coefficient (ADC) of water on tendon while in the linear region show that water has an increased ADC relative to tendon in the resting state (57). Water was extruded from the tendon during these experiments, which clearly explains the reports of water loss from both static and cyclical load of tendons and ligaments (58,59). Early experiments by Elden (60) also showed that one can change the slope of the linear region by exchanging isopropanol for water as the polar solvent dielectric. The mechanical response of native tendon is in large part determined by the energetics of the removal of water from the hydrophilic surfaces of the collagen molecule, as described by the hydration model. Mechanical properties are modulated by age and diabetes by cross-linking collagen (56) through enzymatic and nonenzymatic covalent bonding mechanisms that affect water content.

MR RELAXATION DEPENDENCE ON STRUCTURAL HYDRATION

T1—Spin Lattice Relaxation

The molecular model of collagen hydration allows one to test the collagen hydration model and provides a molecule with which to validate the NMR titration method for evaluating the hydration of less well characterized proteins or complex tissue mixtures. Zimmerman and Brittin (61) showed that fast exchange of protons between water fractions could explain the variation of T1

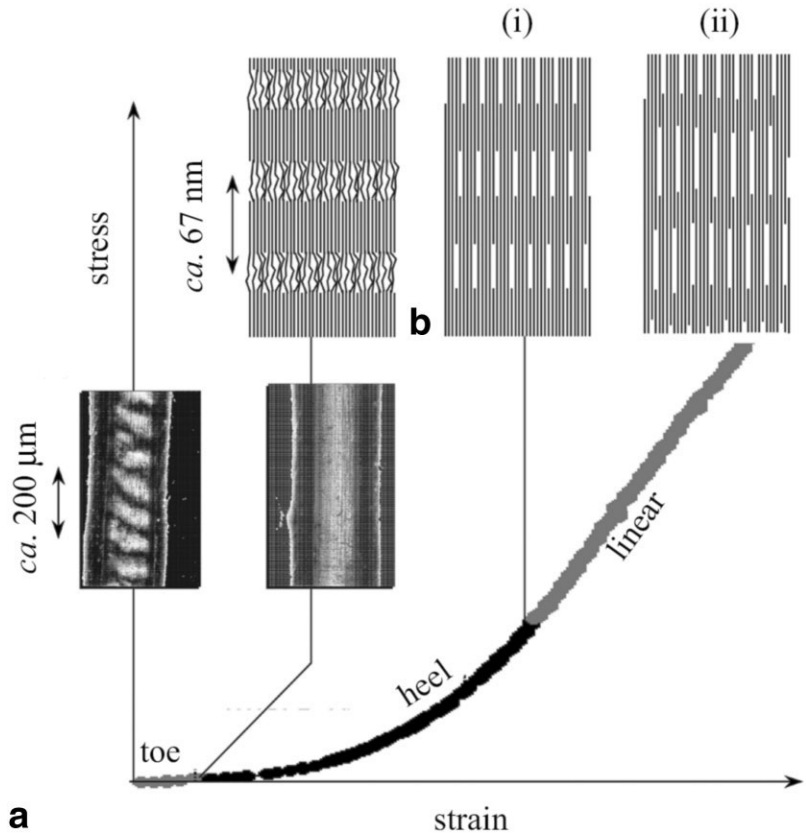

Figure 15. Initially, small stress on tendon causes a large increment in strain = $\Delta l/l_o$ in the toe region due to the elimination of wave-like crimps (**a**). The slope increase in the heel region as the gap region is stretched (**b**), while in the linear region (i–ii) the collagen molecule is stretched (92) and water oozes from the tendon. Removal of hydration prior to experiment causes shrinkage and complete elimination of the toe and heel regions, resulting in a linear stress-strain relationship and increased slope (93). Reprinted from Puxkandl R, Zizak I, Paris O, et al. Viscoelastic properties of collagen: synchrotron radiation investigations and structural model. Philos Trans R Soc Lond B Biol Sci 2002;357:191–197, with permission.

with concentration of water on a silica gel. Fullerton and colleagues (62) used these concepts to develop an NMR titration method to identify and characterize water compartments on hydrated proteins, but they lacked a molecular model with which to validate the measurement method. More recently, this group applied the method to the study of bovine tendon (43) with the assumption that the dry mass was equivalent to the collagen mass. These experiments, done at 10 MHz, provide adequate separation of compartmental relaxation rates to validate the collagen hydration model, as shown in Fig. 16. The peak in spin-lattice relaxation rate at $h = 0.263$ g/g shows that the relaxation sink for the entire water/collagen system is primary hydration of polar sites on the protein main chain. The remainder of the curve is less emphatic proof of the collagen hydration model.

T2—Spin-Spin Relaxation

Berendsen (1) was the first to notice the large orientational dependence of the T2 relaxation time on tendon. Fullerton et al (3) cautioned that this dependence could cause a factor of 6 variation in the spin-echo signal in clinical MRI. Attempts to explain variation by multicomponent relaxation using exchange models are useful but inconclusive due to the lack of a molecular model, and dependence on critical experimental factors in the pulse sequences (4–6,63). The group led by Navon used a double-quantum technique to study fiber orientation in tendon and confirm anisotropy of residual dipole coupling due to bound water on the collagen (64–67). Other groups used MR diffusion measurements to demonstrate water self-diffusion anisotropy on tendon (57,68). Wellen et al (68) showed that water was freed from the tendon under stress to increase both the axial and transverse ADC. The change in ADC with orientation was related to greater tortuosity in the axial direction relative to the more open paths along the tendon axis. Fechete et al (69) identified two diffusion components, with the slow fraction accounting for approximately 25% of the water, and the fast component accounting for 75%. These observations are consistent with the collagen hydration model and geometry. Krasnosselskaia et al (14) used orientational analysis of the free induction decay (FID) of the ^{1}H NMR water signal of bovine tendon to show that residual dipole coupling causes a 6:1 variation in signal intensity with orientation. As shown in Fig. 17, the orientational dependence is primarily due to dipole coupling, while the smaller orientationally independent water fraction is disordered water associated with cross-links in the gap region between collagen molecules. Multiexponential decay is thought to be due to fast exchange between the larger orientationally restricted water compartment (geometrically 89% of total volume) and the smaller disordered water fraction in the gaps (geometrically 11%). The ratio of these volumes $0.54D/(5 \times 0.46D + 4 \times 0.54D) = 12.4\%$ is close to the measured ratio of $1/6 = 16\%$.

MR Image Contrast Dependence on Structural Hydration

The imaging experiments of Rahal et al (70) demonstrate the structural source of MR orientational con-

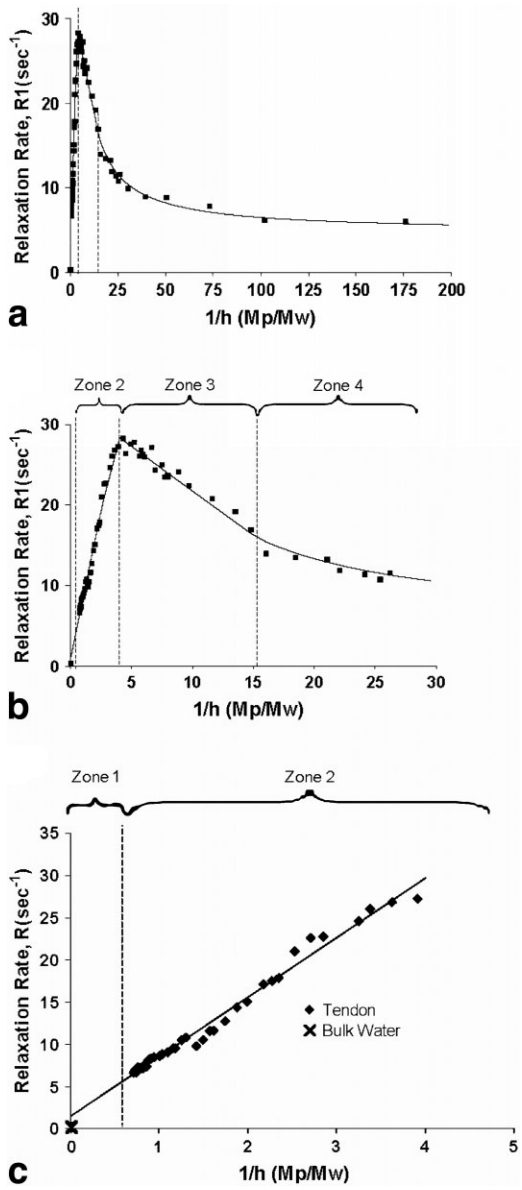

Figure 16. Zonal analysis of the T1 relaxation rate vs. the reciprocal of hydration $1/h$ as predicted by the collagen hydration model confirms both the hydration limits of the compartments as well as motional slowing of water compartments in the first monolayer (43). A multisegment nonlinear least-squares regression fit ($R^2 = 0.9916$) for $N = 74$ measurements over the entire range of hydration from native to completely dry protein residue demonstrates the capacity of the collagen hydration model to describe spin lattice relaxation of tendon. **a:** The entire range of experiments. **b:** Data from zone 3. **c:** Data from zone 2. Each zone is identified as a range of hydrations by the collagen model as follows: zone 1: $h > 1.584$ g water/g dry mass; zone 2: 1.584 g/g $> h > 0.264$ g/g; zone 3: $0.264 > h > 0.0658$ g/g; and zone 4: $h < 0.0658$ g/g. Reprinted from Fullerton GD, Nes E, Amurao M, Rahal A, Krasnosselskaia L, Cameron I. NMR method to characterize multiple water compartments on mammalian collagen. Cell Biol Int 2006;30:66–73, with permission from Elsevier.

trast variation most graphically. These images of bovine tendon samples aligned either with the magnetic field or at the MA 55° relative to B_0 demonstrate the six-fold higher intensity of signal at the MA, as shown in Fig. 18.

CLINICAL APPLICATIONS OF THE MA EFFECT

The molecular characteristics of the collagen–water interactions described above are responsible for the very low signal intensity that originates from highly oriented collagenous tissues when fibers are parallel to the magnetic field. Signal from these tissues is even lower than free-water signal in T1-weighted sequences. The gradual increase of signal intensity on changing orientation to a peak at the MA is secondary to a gradual loss of dipolar interactions of water molecules that become "visible" near the MA and result in a net increase of T2/T2*. This is a characteristic of highly oriented collagenous tissue and is not observed in focal lesions that replace or disrupt collagen. Figure 18 demonstrates the MA effect on samples of bovine tendon, and the plots in Fig. 19 are measured signal intensity in tendon at increasing angles to B_0.

In pathologic conditions, there is loss of organized collagen structure, with focal increased free fluid, mucinous vacuoles, cellular debris, and fibrin, and disorganization of orientation of collagen fibers. These substances will not follow the signal characteristics of collagen and will demonstrate higher signal than normal collagen on all MRI sequences when parallel to B_0. The MA phenomenon also explains why signal from organized collagen at the MA is usually higher than signal from pathologic conditions in MRI sequences that are sensitive to the MA effect.

The musculoskeletal imaging literature deals with the MA phenomenon in different ways. Most authors consider the increased signal from tendon as an artifact that may simulate tendinosis. Others have tried to incorporate the effect into techniques that may aid in depicting the normal anatomy, identifying early tendinous pathology, and detecting contrast enhancement.

Bright Tendinosis Lesions Have a Molecular Collagen Source

A number of clinical studies have demonstrated increased signal intensity in tendon secondary to chronic tendinosis (71–75). The molecular description of the process involves two factors. Most superconducting MR imagers have magnetic fields parallel to the table and the patient's body axis. Normal tendons are black when parallel to the magnetic field. Tendon injury or degeneration causes the release of matrix-metalloproteinases (MMPs) or collagenases used by the body to break down damaged collagen and allow restructuring of the extracellular matrix during damage cleanup and repair. The regions under repair lack normal collagen structure and become disordered. Such lesions are bright on the black background of normal tendon, as shown by Rahal et al in Figure 18 (70). The resultant lesions are a result of clipping and destruction of the collagen molecular structure.

Increased Signal by Imaging at the MA

Different methods have been used to enhance anatomic depiction of tendons and/or improve detection of disease processes. The increased signal in tendon

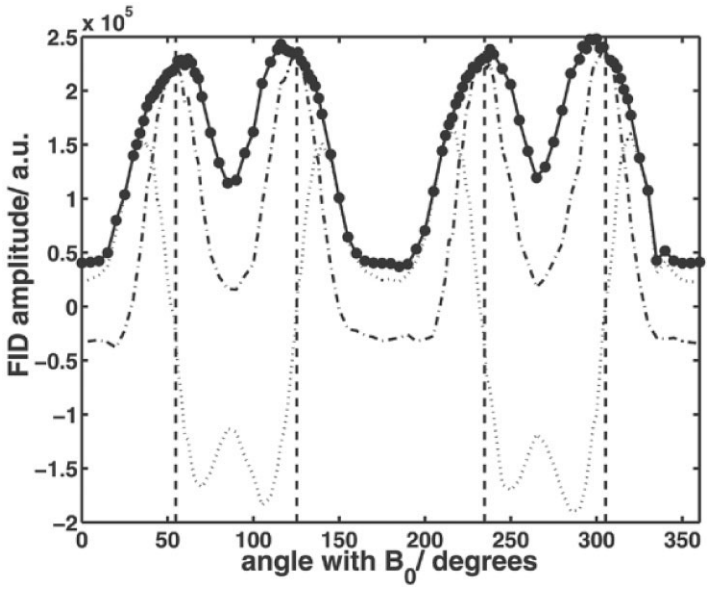

Figure 17. Measured orientation dependence of the FID amplitude for bovine tendon is plotted with signal in the real channel (dash-dot line), imaginary channel (dotted line), and absolute value (solid line). The absolute value shows the 6:1 variation with orientation, while the real and imaginary components show phase shift caused by residual dipole coupling (780-Hz shift). The small orientationally independent fraction is consistent with the size of the molecular gap region. Measured frequency and phase shifts are consistent with bulk susceptibility effect due to the geometry of the cavity (see Ref. 14 for details). Reprinted from Krasnosselskaia L, Fullerton GD, Dodd SJ, Cameron IL. Water in tendon: Orientational analysis of the free induction decay. Magn Reson Med 2005;54:280–288, with permission from Wiley-Liss, Inc., a subsidiary of John Wiley & Sons Inc.

at the MA has been used purposely in different settings (7–10,76) to improve visualization of tendinous structures, detect contrast enhancement in tendinosis, and depict digital tendon anatomy. These clinical techniques rely on the structural integrity of normal collagen in the tendon to eliminate dipole-dipole coupling when the molecule is aligned at 55°. They are limited to the few structures that can be repositioned in the MRI bore, such as the Achilles, patellar, and digital tendons.

Increased Tendon SNR and CNR Using Very Short TE

With the use of gradient-echo (GRE) sequences that employ the lowest TE values available in clinical systems (as low as 1–2 msec with modern gradient systems), it is possible to detect signal from tendon and other structures with short T2/T2*. This clinical method endeavors to minimize the effects of dipole-dipole coupling of water molecules on collagen by re-

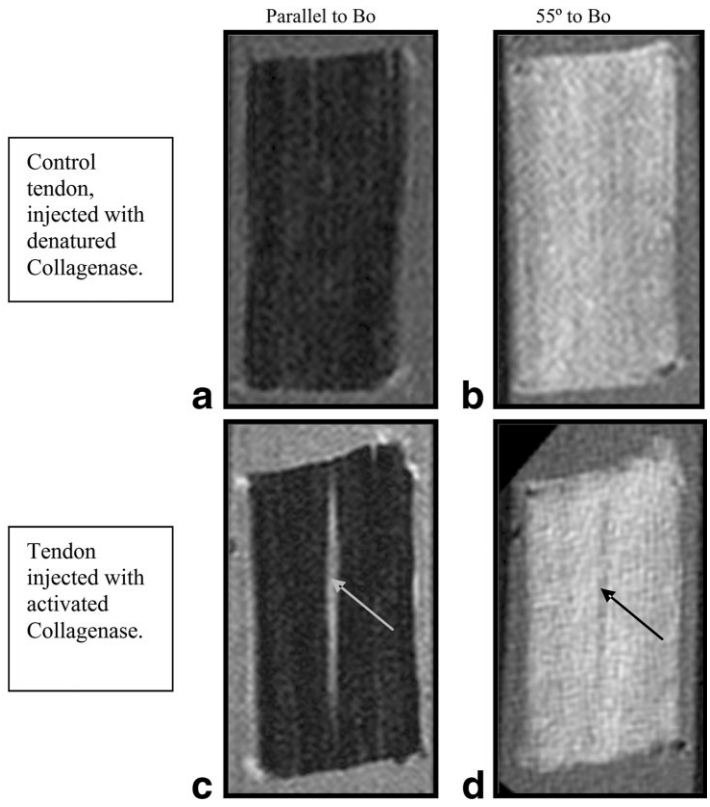

Figure 18. In vitro MR images of bovine deep flexor tendon suspended in PBS by Rahal and colleagues (70) demonstrate a six-fold increase in signal intensity between (**a**) parallel to B_0 and (**b**) at the MA of 55°. **c:** Injection of 0.2 mL of collagenase in the center of the tendon causes enzymatic digestion of the collagen molecular structure (see arrows). The suppression of MR signal at the parallel orientation is eliminated in the digested region, where the molecular structure is disrupted causing a bright signal from the lesion. **d:** All water is visible at the MA, but the lesion becomes dark with slight decrease in signal due to increased T1 resulting from increased water content. This increase is caused by osmotic influx due to the increased number of small molecular fragments. Injections of 0.2 mL of distilled water, saline, or inactivated collagenase (heated to 90°C to denature the protein) caused no visible lesion, and were all identical to the denatured collagenase control images shown at the top (alternatives not shown for clarity). The influence of active collagenase on image contrast simulates clinical observations of tendinosis-like lesions.

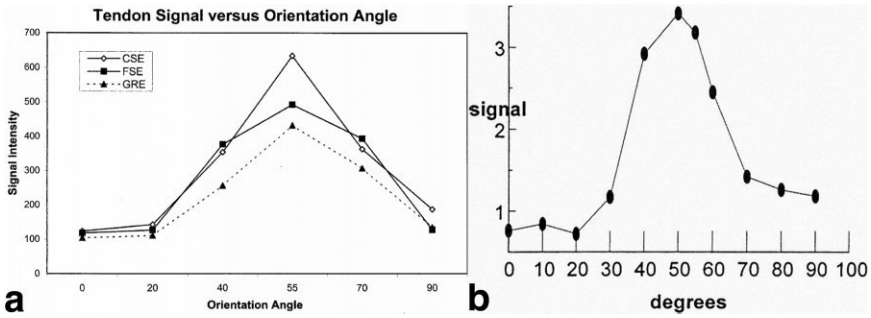

Figure 19. Plots of MR signal intensity measured for ROIs centered on human tendon images as a function of orientation show the same orientational dependence as the in vitro results shown in Fig. 16. **a:** Li and Mirowitz (84) showed that CSE, FSE, and GRE have similar orientational variation in signal intensity for tendon at different orientations from B_0 due to the collagen. **b:** Bydder (7) showed increased signal in tendon at angles >20° from B_0, which peaks at 55°. Note that the signal does not decrease to baseline at 90° due to the proximity of the next MA peak at 125.3° (180° minus 54.7°). Reprinted from Bydder GM. New approaches to magnetic resonance imaging of intervertebral discs, tendons, ligaments, and menisci. Spine 2002;27:1264–1268, with permission of Lippincott, Williams & Wilkins and Li T, Mirowitz SA. Manifestation of magic angle phenomenon: comparative study on effects of varying echo time and tendon orientation among various MR sequences. J Magn Reson Imaging 2003;21: 741–744, with permission from Wiley-Liss, Inc., a subsidiary of John Wiley & Sons Inc.

trieving the signal before excessive T2* decay reduces the signal below the limit of useful contrast. The method has been used alone as well as in combination with positioning at or near the MA (12).

Highest SNR and CNR at Parallel Orientation Using Ultrashort TE (UTE) Imaging

UTE imaging methods use gradient sequences that read out the FID immediately after the RF pulse to detect signal from structures with very short T2/T2*, such as tendon, using TEs on the order of 50–100 msec (12,77). This technique is clinically the most promising because it produces high signal in tendon without the need to position the structure of interest at the MA. It has proven useful for detecting contrast enhancement in tendon, cartilage, ligaments, enthesis, and cortical bone. However, this technique remains sensitive to increased signal at the MA in the same way as traditional MRI sequences (7,8,12,13,77).

Orientational Artifacts Reduced by Careful Positioning

The 600% contrast variation with a change of orientation of only 55° leads to great potential for misinterpreting "orientational artifacts" as lesions. Multiple articles have commented on the increased intensity of tendons when oriented close to the MA as a pitfall in musculoskeletal imaging. This increased signal is expected in specific locations secondary to the anatomic orientation in the body that places them close to the MA. Examples include the supraspinatus and infraspinatus tendons close to the humeral attachment (78), the proximal aspect of the patellar tendon (75,79), and the peroneal tendons below the level of the ankle (80). Specific attention is recommended by these authors to correct positioning of patients during MRI in a way that prevents these specific tendons from being oriented close to the MA. Recent MRI protocols avoid the previously recommended 10–15° of flexion and external rotation for knee MRI (75), and traditional protocols for ankle/foot imaging recommend about 20° plantar flexion for avoiding the MA in peroneal and other ankle tendons (80–82).

An important observation is that increased signal intensity in tendon due to the MA effect peaks at 55°; however, signal increases gradually from angles as low as 20°. The signal intensity does not return to baseline at 90° because of averaging of the two Lorentzian MA peaks at 54.7° and 125.3° (180° minus 54.7°), as observed in Figs. 17 and 19. Figure 18 shows that the orientational variation of signal in tendon by MRI is identical to that obtained by NMR in Fig. 17. This means that signal is increased from baseline in all tendons that are not oriented within ±20° to B_0. The increased signal of normal tendon at the MA in clinical imaging is shown in Fig. 20.

MRI Protocols to Reduce the Risk of MA Artifacts

Clinical protocols have also tried to eliminate the MA effect in tendons that are not parallel to B_0 given the sometimes difficult positioning of body parts. The MA effect is less intense or absent in sequences with longer TE. Critical TE values were defined as 37 msec for T1- and PD-weighted sequences in experimental work on explanted bovine tendon by Peh and Chan (83). Similar work on explanted tendon by Li and Mirowitz (84) showed critical TE values of 40, 70, and 30 msec on conventional spin-echo (CSE), fast spin-echo (FSE), and GRE techniques, respectively. One clinical study by Zurlo et al (85) showed that larger flip angles decrease the MA effect in GRE sequences especially at TE <30 ms, and a decreased MA effect is observed with a flip angle of 70° as compared to 20°.

Correlation of MRI Sequences to Limit the Artifact Error Rate

The finding of increased signal intensity in tendon on sequences with low TE (T1-weighted, PD-weighted, or GRE sequences) is only considered significant by some authors if the increased signal is found concurrently in long-TE sequences (i.e., T2-weighted sequences with or

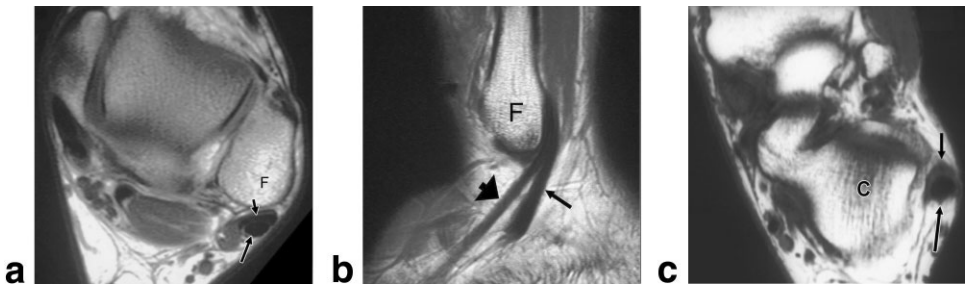

Figure 20. This clinical study adapted from Wang et al (80) shows the difficulty of identifying orientational effects on tendon when viewed with (**a**) axial vs. (**b**) sagittal slices. These T1-weighted MR images demonstrate normal peroneus brevis (short arrow) and peroneus longus (long arrow) tendons descending posterior to the lateral malleolus (F). The peroneus brevis tendon is mildly crescentic in configuration on the axial image. **c:** The axial T1-weighted MR image obtained with the patient's ankle in dorsiflexion shows MA phenomenon on the peroneus brevis tendon with increased signal intensity (short arrow), a finding that simulates disease. On an axial image obtained with the ankle at about 20° plantar flexion (not shown), the tendon had normal low signal intensity. The long arrow indicates the peroneus longus tendon, C = calcaneus. Careful reference to magnetic field direction is important when considering image contrast in all planes. Adapted from Wang X-T, Rosenberg ZS, Mechlin MB, Schweitzer ME. Normal variants and diseases of the peroneal tendons and superior peroneal retinaculum: MR imaging features. Radiographics 2005;25:587–602.

without fat suppression) (80,86,87). Otherwise, they consider the finding nonspecific and probably due to the MA effect.

Importance of Tendon Orientation When Reading Alternative Views

The complexity of remaining aware of magnetic field orientation relative to collagen orientation in joints, ligaments, and tendons is shown in Fig. 20. Imaging at the MA improves visualization of tendinous structures, but changes when structures such as the Achilles, patellar, and digital tendons are repositioned in the MRI bore. The reader must remain aware of these effects even when switching from axial to sagittal, coronal, or even random plane orientation through the same structures. A clinical example of loss of the MA effect in a tendinosis-like lesion is shown in Fig. 21.

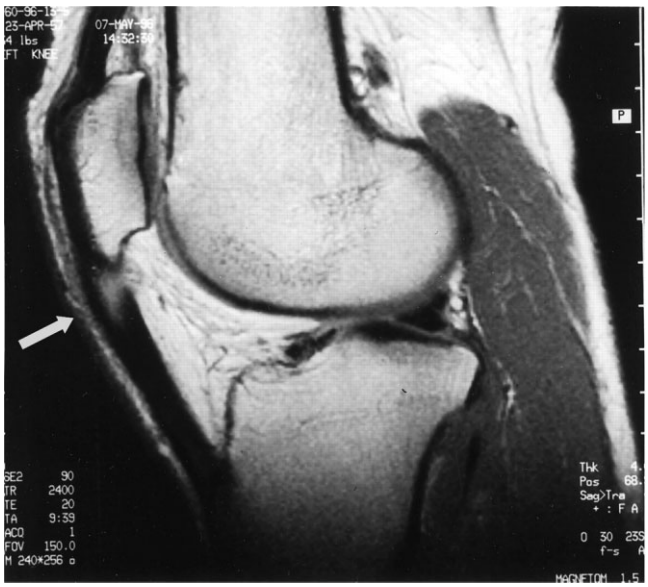

Figure 21. Clinical example of tendinosis shows black tendon due to short T2* when the tendon is aligned parallel to B_0, with a bright lesion where the alignment of water molecules perpendicular to the tendon axis is destroyed by collagen digestion. The T1-weighted sagittal image of the knee shows increased signal intensity and increased diameter (white arrow) in the patellar tendon of a long-distance runner with a clinical diagnosis of tendinosis. The mechanism of increased signal intensity is related to disruption of collagen integrity by collagenases (MMPs) in the degeneration and renewal process seen in tendinosis. Adapted from Shalaby M, Almekinders LC. Patellar tendinitis: the significance of magnetic resonance imaging findings. Am J Sports Med 1999;27:345–349, with permission from Sage Publications Inc.

CONCLUSIONS

The preferential orientation of the electric dipole of the water molecule in the tendon transverse plane causes orientational MRI (OMRI) behavior, i.e., the MA effect. The polarization of the water molecules reduces the electrostatic energy in fields generated between adjacent positive amide and negative carbonyl groups on the main chain of the collagen molecule to form the energy well that binds water to the protein. The positive and negative partial electron charges on the protein are caused by the exceptional electronegative character of the nitrogen and oxygen atoms that are covalently bound in the protein molecule. Anisotropic rotation of the bound water molecules causes accumulation of phase shift due to dipole coupling between the hydrogen nuclei (protons) on the water molecule. Orientation of tendons at the MA 54.7° relative to B_0 reduces the dipole coupling to zero, which causes all water-related protons to resonate at the same frequency and increases the effective T2/T2*. A growing body of clinical literature demonstrates that although OMRI can be an annoying source of MA artifact, it also has potential to provide a useful new contrast mechanism, especially for studies of the extracellular matrix. This is especially attractive when one considers the widespread distribution of collagen in the body, and that nearly one-third of human protein comes from this single family of triple helix molecules.

ACKNOWLEDGMENTS

Financial support is acknowledged from the Malcolm Jones Distinguished Professorship (GDF) and special-

ized MR imaging assistance under the general Research Agreement with Philips Medical Systems.

REFERENCES

1. Berendsen HJ. Nuclear magnetic resonance study of collagen hydration. J Chem Phys 1962;16:3297–3305.
2. Berendsen HJ. Hydration structure of fibrous macromolecules. Ann NY Acad Sci 1965;125:365–379.
3. Fullerton GD, Cameron IL, Ord VA. Orientation of tendons in the magnetic field and its effect on T2 relaxation times. Radiology 1985; 155:433–435.
4. Henkelman RM, Stanisz GJ, Kim JK, Bronskill MJ. Anisotropy of NMR properties of tissues. Magn Reson Med 1994;32:592–601.
5. Peto S, Gillis P. Fiber-to-field angle dependence of proton nuclear magnetic relaxation in collagen. Magn Reson Imaging 1990;8:705–712.
6. Peto S, Gillis P, Henri VP. Structure and dynamics of water in tendon from NMR relaxation measurements. Biophys J 1990;57: 71–84.
7. Bydder GM. New approaches to magnetic resonance imaging of intervertebral discs, tendons, ligaments, and menisci. Spine 2002; 27:1264–1268.
8. Gatehouse PD, Bydder GM. Magnetic resonance imaging of short T2 components in tissue. Clin Radiol 2003;58:1–19.
9. Marshall H, Howarth C, Larkman DJ, Herlihy AH, Oatridge A, Bydder GM. Contrast-enhanced magic-angle MR imaging of the Achilles tendon. AJR Am J Roentgenol 2002;179:187–192.
10. Oatridge A, Herlihy AH, Thomas RW, et al. Magnetic resonance: magic angle imaging of the Achilles tendon. Lancet 2001;358: 1610–1611.
11. Robson MD, Gatehouse PD, Bydder GM, Neubauer S. Human imaging of phosphorus in cortical and trabecular bone in vivo. Magn Reson Med 2004;51:888–892.
12. Robson MD, Gatehouse PD, Bydder M, Bydder GM. Magnetic resonance: an introduction to ultrashort TE (UTE) imaging. J Comput Assist Tomogr 2003;27:825–846.
13. Robson MD, Gatehouse PD, So PW, Bell JD, Bydder GM. Contrast enhancement of short T2 tissues using ultrashort TE (UTE) pulse sequences. Clin Radiol 2004;59:720–726.
14. Krasnosselskaia L, Fullerton GD, Dodd SJ, Cameron IL. Water in tendon: orientational analysis of the free induction decay. Magn Reson Med 2005;54:280–288.
15. Rich A, Crick F. The molecular structure of collagen. J Mol Biol 1961;3:483.
16. Rich A, Crick F. The structure of collagen. Nature (Lond) 1955;176: 176.
17. Ramachandran GN, Kartha G. Structure of collagen. Nature (Lond) 1954;174:269.
18. Ramachandran GN, Kartha G. Structure of collagen. Nature (Lond) 1955;176:593.
19. Ramachandran GN. Stereochemistry of collagen. Int J Pept Protein Res 1988;31:1–16.
20. Ramachandran GN, Chandrasekharan R. Interchain hydrogen bonds via bound water molecules in the collagen triple helix. Biopolymers 1968;6:1649–1658.
21. Ramachandran GN. Structure of collagen at the molecular level. In: Ramachandran GN, editor. Treatise on collagen. Vol. 1. New York: Academic Press; 1967. p 103–183.
22. Ramachandran GN, Ramakrishnan C. Molecular structure. In: Ramachandran GN, Reddi AH, editors. Biochemistry of collagen. New York: Plenum Press; 1976. p 45–84.
23. Yee RY, Englander SW, Von Hippel PH. Native collagen has a two-bonded structure. J Mol Biol 1974;83:1–16.
24. Burjanadze TV. Thermodynamic substantiation of water-bridged collagen structure. Biopolymers 1992;32:941–949.
25. Berisio R, Vitagliano L, Mazzarella L, Zagari A. Crystal structure of the collagen triple helix model [(Pro-Pro-Gly)]. Protein Sci 2002;11: 262–270.
26. Jeffrey GA, Saenger W. Hydrogen bonding in biological structures. Vol. 1. Berlin: Springer Verlag; 1991. p 1–569.
27. Makhatadze GI, Privalov PL. Contribution of hydration to protein folding thermodynamics. I. The enthalpy of hydration. J Mol Biol 1993;232:639–659.
28. Lim VI. A novel structural model for collagen: water-carbonyl helix. FEBS Lett 1981;132:1–5.
29. Fullerton GD, Nes E, Amarau M, Rahar A, Krasnosselskaia L. Cameron IL. An NMR method to characterize multiple water compartments on mammalian collagen. Cell Biol Int 2006;30:66–73.
30. Fullerton GD, Amurao MR. Evidence that collagen and tendon have monolayer water coverage in the native state. Cell Biol Int 2006;30: 56–65.
31. Bella J, Brodsky B, Berman HM. Hydration structure of a collagen peptide. Structure 1995;3:893–906.
32. Bella J, Brodsky B, Berman HM. Disrupted collagen architecture in the crystal structure of a triple-helical peptide with a Gly—>Ala substitution. Connect Tissue Res 1996;35:401–406.
33. Bella J, Eaton M, Brodsky B, Berman HM. Crystal and molecular structure of a collagen-like peptide at 1.9 A resolution. Science 1994;266:75–81.
34. Kramer RZ, Bella J, Brodsky B, Berman HM. The crystal and molecular structure of a collagen-like peptide with a biologically relevant sequence. J Mol Biol 2001;311:131–147.
35. Kramer RZ, Venugopal MG, Bella J, Mayville P, Brodsky B, Berman HM. Staggered molecular packing in crystals of a collagen-like peptide with a single charged pair. J Mol Biol 2000;301:1191–1205.
36. Kramer RZ, Vitagriano L, Bella J, et al. X-ray crystallographic determination of a collagen-like peptide with the repeating sequence (Pro-Pro-Gly). J Mol Biol 1998;280:623–638.
37. Miller S, Janin J, Lesk AM, Chothia C. Interior and surface of monomeric proteins. J Mol Biol 1987;196:641–656.
38. Miller S, Janin J, Lesk AM, Chothia C. The accessible surface area and stability of oligomeric proteins. Nature 1987;328:834–836.
39. Leikin S, Parsegian VA, Yang W, Walrafen GE. Raman spectral evidence for hydration forces between collagen triple helices. Proc Natl Acad Sci USA 1997;94:11312–11317.
40. Susi H, Ard JS, Carrol RJ. The infrared sectrum and water binding of collagen as a function of relative humidity. Biopolymers 1971; 10:1597–1604.
41. Luescher M, Ruegg M, Schindler P. Effect of hydration upon the thermal stability of tropocollagen and its dependence on the presence of neutral salts. Biopolymers 1974;13:2489–2503.
42. Zhang J, Zhang Z, Zhang W, Fu Y, Ye G, Nin Z. Hydration and thermotransition of collagen fibre. In: Pullman A, Vasilescu V, Packer L, editors. Water and ions in biological systems. New York: Plenum; 1985. p 197–214.
43. Fullerton GD, Nes E, Amurao M, Rahal A, Krasnosselskaia L, Cameron IL. An NMR method to characterize multiple water compartments on mammalian collagen. Cell Biol Int 2006;30:66–73.
44. Privalov PL. Stability of proteins. Proteins which do not present a single cooperative system. Adv Protein Chem 1982;35:1–104.
45. Miles CA, Ghelashvili M. Polymer-in-a-box mechanism for the thermal stabilization of collagen molecules in fibers. Biophys J 1999; 76:3243–3252.
46. Sasaki N, Shiwa S, Yagihara S, Hikichi K. X-ray diffraction studies on the structure of hydrated collagen. Biopolymers 1983;22:2539–2547.
47. Fullerton GD, Kanal KM, Cameron IL. On the osmotically unresponsive water compartment in cells. Cell Biol Int 2006;30:74–77.
48. Fullerton GD, Kanal KM, Cameron IL. Osmotically unresponsive water fraction on proteins: non-ideal osmotic pressure of bovine serum albumin as a function of pH and salt concentration. Cell Biol Int 2006;30:86–92.
49. Parsegian VA, Rand RP, Fuller NL, Rau DC. Osmotic stress for the direct measurement of intermolecular forces. In: Packer L, editor. Methods in enzymology 127: biomembranes part O (protons and water: structure and translocation). Orlando, FL: Academic Press; 1986. p 400–416.
50. Kuznetsova N, Leikin S. Does the triple helical domain of type I collagen encode molecular recognition and fiber assembly while telopeptides serve as catalytic domains? Effect of proteolytic cleavage on fibrillogenesis and on collagen-collagen interaction in fibers. J Biol Chem 1999;274:36083–36088.
51. Kuznetsova N, Rau DC, Parsegian VA, Leikin S. Solvent hydrogen-bond network in protein self-assembly: solvation of collagen triple helices in nonaqueous solvents. Biophys J 1997;72:353–62.
52. Leikin S, Parsegian VA. Temperature-induced complementarity as a mechanism for biomolecular assembly. Proteins 1994;19:73–76.
53. Leikin S, et al. Hydration forces. Ann Rev Phys Chem 1993;44:369.
54. Ramachandran GN. In: Structure of collagen at the molecular level. Ramachandran GN, editor. Treatise on collagen. Volume 1. New York: Academic Press; 1967. p 143.

55. Kjaer M. Role of extracellular matrix in adaptation of tendon and skeletal muscle to mechanical loading. Physiol Rev 2004;84:649–98.
56. Kato YP, Christiansen DL, Hahn RA, Shieh SJ, Goldstein JD, Silver FH. Mechanical properties of collagen fibres: a comparison of reconstituted and rat tail tendon fibres. Biomaterials 1989;10:38–42.
57. Han S, Gemmell SJ, Helmer KG. Changes in ADC caused by tensile loading of rabbit achilles tendon: evidence for water transport. J Magn Reson 2000;144:217–227.
58. Chimich D, Shrive N, Frank C, Marchuk L, Bray R. Water content alters viscoelastic behaviour of the normal adolescent rabbit medial collateral ligament. J Biomech 1992;25:831–837.
59. Hannafin JA, Arnoczky SP. Effect of cyclic and static tensile loading on water content and solute diffusion in canine flexor tendons: an in vitro study. J Orthop Res 1994;12:350–356.
60. Elden HR. Hydration of connective tissue and tendon elasticity. Biochim Biophys Acta 1964;79:592–599.
61. Zimmerman JR, Brittin WE. Nuclear magnetic resonance in multiple phase systems: life time of a water molecule in an absorbing phase on silica gel. J Phys Chem 1957;6:1328–1333.
62. Fullerton GD, Ord VA, Cameron IL. An evaluation of the hydration of lysozyme by an NMR titration method. Biochem Biophys Acta 1986;869:230–246.
63. Rubenstein JD, Kim JK, Morova-Protzner I, Stanchev PL, Henkelman RM. Effects of collagen orientation on MR imaging characteristics of bovine articular cartilage. Radiology 1993;188:219–226.
64. Eliav U, Navon G. A study of dipolar interactions and dynamic processes of water molecules in tendon by 1H and 2H homonuclear and heteronuclear multiple-quantum-filtered NMR spectroscopy. J Magn Reson 1999;137:295–310.
65. Eliav U, Navon G. Multiple quantum filtered NMR studies of the interaction between collagen and water in the tendon. J Am Chem Soc 2002;124:3125–3132.
66. Fechete R, Demco DE, Blumich B, Eliav U, Navon G. Anisotropy of collagen fiber orientation in sheep tendon by 1H double-quantum-filtered NMR signals. J Magn Reson 2003;162:166–175.
67. Navon G, Shinar H, Eliav U, Seo Y. Multiquantum filters and order in tissues. NMR Biomed 2001;14:112–132.
68. Wellen J, Helmer KG, Grigg P, Sotak H. Application of porous-media theory to the investigation of water ADC changes in rabbit Achilles tendon caused by tensile loading. J Magn Reson 2004;170:49–55.
69. Fechete R, Demco DE, Eliav U, Blumich B, Navon G. Self-diffusion anisotropy of water in sheep Achilles tendon. NMR Biomed 2005;18:577–586.
70. Rahal A, Chhaya SA, Garcia GM, Heim-Hall J, Fullerton GD. High frequency ultrasound and MR imaging of tendons: evaluation of ex vivo models of normal and injured bovine tendon with histopathologic correlation. In: Proceedings of the 91st Annual Meeting of RSNA, Chicago, IL, USA, 2005.
71. Wang XT, Rosenberg ZS, Mechlin MB, Schweitzer ME. Normal variants and diseases of the peroneal tendons and superior peroneal retinaculum: MR imaging features. Radiographics 2005;25:587–602.
72. Astrom M, Gentz CF, Nilsson P, Rausing A, Sjoberg S, Westlin N. Imaging in chronic achilles tendinopathy: a comparison of ultrasonography, magnetic resonance imaging and surgical findings in 27 histologically verified cases. Skeletal Radiol 1996;25:615–620.
73. Shalabi A. Magnetic resonance imaging in chronic Achilles tendinopathy. Acta Radiol Suppl 2004:1–45.
74. Shalabi A, Kristoffersen-Wiberg M, Aspelin P, Movin T. MR evaluation of chronic Achilles tendinosis. A longitudinal study of 15 patients preoperatively and two years postoperatively. Acta Radiol 2001;42:269–76.
75. Shalaby M, Almekinders LC. Patellar tendinitis: the significance of magnetic resonance imaging findings. Am J Sports Med 1999;27:345–349.
76. Oatridge A, Herlihy A, Thomas RW, et al. Magic angle imaging of the achilles tendon in patients with chronic tendonopathy. Clin Radiol 2003;58:384–388.
77. Robson MD, Benjamin M, Gishen P, Bydder GM. Magnetic resonance imaging of the Achilles tendon using ultrashort TE (UTE) pulse sequences. Clin Radiol 2004;59:727–735.
78. Wright T, Yoon C, Schmit BP. Shoulder MRI refinements: differentiation of rotator cuff tear from artifacts and tendonosis, and reassessment of normal findings. Semin Ultrasound CT MR 2001;22:383–395.
79. Karantanas AH, Zibis AH, Papanikolaou N. Increased signal intensity on fat-suppressed three-dimensional T1-weighted pulse sequences in patellar tendon: magic angle effect? Skeletal Radiol 2001;30:67–71.
80. Wang X-T, Rosenberg ZS, Mechlin MB, Schweitzer ME. Normal variants and diseases of the peroneal tendons and superior peroneal retinaculum: MR imaging features. Radiographics 2005;25:587–602.
81. Lamm BM, Myers DT, Dumbek M, Mendicino RW, Catanzariti AR, Saltrick K. Magnetic resonance imaging and surgical correlation of peroneus brevis tears. J. Foot Ankle Surg. 2004;2004:30–36.
82. Saxena A, Wolf SK. Peroneal tendon abnormalities. A review of 40 surgical cases. J Am Podiatr Med Assoc 2003;93:272–282.
83. Peh WC, Chan JH. The magic angle phenomenon in tendons: effect of varying the MR echo time. Br J Radiol 1998;71:31–36.
84. Li T, Mirowitz SA. Manifestation of magic angle phenomenon: comparative study on effects of varying echo time and tendon orientation among various MR sequences. Magn Reson Imaging 2003;21:741–744.
85. Zurlo JV, Blacksin MF, Karimi S. The influence of flip angle on the magic angle effect. Skeletal Radiol 2000;29:593–596.
86. Schweitzer ME, Karasick D. MR imaging of disorders of the Achilles tendon. AJR Am J Roentgenol 2000;175:613–625.
87. Haims AH, Schweitzer ME, Patel RS, Hecht P, Wapner KL. MR imaging of the Achilles tendon: overlap of findings in symptomatic and asymptomatic individuals. Skeletal Radiol 2000;29:640–645.
88. Leikin S, Rau DC, Parsegian VA. Direct measurement of forces between self-assembled proteins: temperature-dependent exponential forces between collagen triple helices. Proc Natl Acad Sci USA 1994;91:276–280.
89. Kuznetsova N, Chi SL, Leikin S. Sugars and polyols inhibit fibrillogenesis of type I collagen by disrupting hydrogen-bonded water bridges between the helices. Biochemistry 1998;37:11888–11895.
90. Berendsen HJ, Migchelsen C. Hydration structure of collagen and influence of salts. Fed Proc 1966;25:998–1002.
91. Silver FH, Freeman JW, Seehra GP. Collagen self-assembly and the development of tendon mechanical properties. J Biomech 2003;36:1529–1553.
92. Puxkandl R, Zizak I, Paris O, et al. Viscoelastic properties of collagen: synchrotron radiation investigations and structural model. Phil Trans R Soc Lond B Biol Sci 2002;357:191–197.
93. Betsch DF, Baer E. Structure and mechanical properties of rat tail tendon. Biorheology 1980;17:83–94.